Cerebral Cortex, August 2016;26: 3553–3562

doi:10.1093/cercor/bhw158
Advance Access Publication Date: 27 May 2016
Original Article

ORIGINAL ARTICLE

Effects of Hypocretin/Orexin and Major Transmitters of Arousal on Fast Spiking Neurons in Mouse Cortical Layer 6B

Anne-Laure Wenger Combremont[1], Laurence Bayer[1,2], Anouk Dupré[1], Michel Mühlethaler[1] and Mauro Serafin[1]

[1]Département des Neurosciences Fondamentales, Centre Médical Universitaire, Genève, Suisse and [2]Centre de Médecine du Sommeil, Hôpitaux Universitaires de Genève, Genève, Suisse

Address correspondence to M. Mühlethaler, C.M.U. Département des Neurosciences Fondamentales, 1 Rue Michel-Servet, 1211 Genève 4, Suisse. Email: michel.muhlethaler@unige.ch

Abstract

Fast spiking (FS) GABAergic neurons are thought to be involved in the generation of high-frequency cortical rhythms during the waking state. We previously showed that cortical layer 6b (L6b) was a specific target for the wake-promoting transmitter, hypocretin/orexin (hcrt/orx). Here, we have investigated whether L6b FS cells were sensitive to hcrt/orx and other transmitters associated with cortical activation. Recordings were thus made from L6b FS cells in either wild-type mice or in transgenic mice in which GFP-positive GABAergic cells are parvalbumin positive. Whereas in a control condition hcrt/orx induced a strong increase in the frequency, but not amplitude, of spontaneous synaptic currents, in the presence of TTX, it had no effect at all on miniature synaptic currents. Hcrt/orx effect was thus presynaptic although not by an action on glutamatergic terminals but rather on neighboring cells. In contrast, noradrenaline and acetylcholine depolarized and excited these cells through a direct postsynaptic action. Neurotensin, which is colocalized in hcrt/orx neurons, also depolarized and excited these cells but the effect was indirect. Morphologically, these cells exhibited basket-like features. These results suggest that hcrt/orx, noradrenaline, acetylcholine, and neurotensin could contribute to high-frequency cortical activity through an action on L6b GABAergic FS cells.

Key words: acetylcholine, arousal, neurotensin, noradrenaline, sleep

Introduction

Fast spiking (FS) cortical neurons are GABAergic interneurons (McCormick et al. 1985; Connors and Gutnick 1990; Ascoli et al. 2008) that have taken an ever increasing importance in our understanding of cortical network activity. Their denomination is based on their characteristic brief action potentials, their firing with little or no adaptation and their ability to reach a high level of activity when depolarized (McCormick et al. 1985; Connors and Gutnick 1990). Early on, most of them were also shown (Kawaguchi and Kubota 1993) to express the calcium-binding protein parvalbumin (PV). Morphologically, FS parvalbumin positive (FS-PV) cells were found to be of only two types, chandelier or basket cells (Povysheva et al. 2013; Inan and Anderson 2014). In an extension of early studies showing that networks of GABAergic cells can generate fast (40 Hz) synchronized oscillations (Whittington et al. 1995), FS-PV cells have now been shown to participate in the production of a high-frequency rhythm ("gamma band oscillation" or GBO) involved in cognitive processes during the waking state (Freund 2003; Cardin et al. 2009; Sohal et al. 2009; Hu et al. 2014; Kim et al. 2015).

This rhythm was shown to be modulated by the waking state, being reduced during slow wave sleep and increased during waking (Maloney et al. 1997) under the influence of the systems of arousal which notably express noradrenaline, acetylcholine, and the neuropeptide hcrt/orx (Jones 2011). GBO was also shown to be promoted by neurotensin, a peptide colocalized in hcrt/orx neurons (Furutani et al. 2013), through an action on basal forebrain cholinergic neurons (Cape et al. 2000).

Among the transmitter pathways implicated in arousal, the hcrt/orx system holds a special status. It is indeed the only one indispensable for maintaining waking as a deficit in the production of hcrt/orx or an alteration of hypocretin/orexin receptors are the only known conditions which result in narcolepsy in animals and humans (for recent reviews on hcrt/orx, see Siegel and Boehmer 2006; Alexandre et al. 2013; Jones and Hassani 2013; Mahlios et al. 2013; Sakurai 2013; de Lecea and Huerta 2014). Underlying the role of hcrt/orx is the presence of its multiple pathways projecting toward the traditional arousal systems as well as to the thalamus and cortex (Peyron et al. 1998). Very significant also are the evidence that hcrt/orx neurons increase their firing during active waking (Lee et al. 2005; Mileykovskiy et al. 2005) and secrete hcrt/orx and glutamate to, respectively, provide on their targets, an integrating input versus an onset signal (Schone et al. 2014). In all the projection areas, hcrt/orx was found to be excitatory on its targets and notably on the adrenergic (Horvath et al. 1999) and cholinergic neurons (Eggermann et al. 2001; Burlet et al. 2002; Ishibashi et al. 2015) of the arousal systems originating from the brainstem and the basal forebrain (for reviews, see Jones 2011; Jones and Hassani 2013).

Beyond its action on the arousal systems, hcrt/orx was also suggested to affect the cerebral cortex more directly. Indeed, of a particular interest was firstly the demonstration that hcrt/orx exerted an action in the thalamus, and that in this structure it targeted specifically, and exclusively, the widespread cortical projection system of the intralaminar and midline nuclei (Bayer et al. 2002). Secondly, it was shown that hcrt/orx directly affected cortical neurons, but again, at that level, it exerted a direct postsynaptic action specifically and exclusively on neurons of a single sublayer, the layer 6b (Bayer et al. 2004), which is thought to exert a widespread action on the overlying cortex through local or distant corticocortical projections (Clancy and Cauller 1999; Clancy et al. 2001; Arimatsu et al. 2003). This layer, a remnant of the subplate (for review, see Kanold and Luhmann 2010), has been shown to persist into adulthood in many species either as a distinct sublayer at the very bottom of the layer 6 or as a collection of scattered neurons (known as "interstitial neurons") located in the white matter of the corpus callosum (Kostovic and Rakic 1980; Reep and Goodwin 1988; Chun and Shatz 1989; Reep 2000; Clancy et al. 2001; Friedlander and Torres-Reveron 2009).

The goal of the present study was thus to identify FS cells in layer 6b of mouse somatosensory cortical slices and determine whether they are sensitive to hcrt/orx as well as to other transmitters associated with high-frequency cortical rhythms such as noradrenaline, acetylcholine, and neurotensin (Jones 2011). Preliminary results have been published in an abstract form (Wenger et al. 2011).

Materials and Methods

Slice Preparation

Brain slices were obtained from juvenile C57Bl/6 mice (Charles River Laboratories, France) and GAD67-GFP (line G42) transgenic mice (courtesy of Dr Alan Carleton, Geneva University, Geneva, Switzerland) from 17 to 21 day old. These transgenic mice express GFP under the control of a GAD67 bacterial artificial chromosome (BAC) clone. In this line, GFP-positive cells selectively express parvalbumin (although only about 50% of the PV neurons express GFP) in the cortex and most of them have been described as FS basket cells (Chattopadhyaya et al. 2004; Xu and Callaway 2009). Mice were treated according to the rules of the Swiss Federal Veterinary Office (approval ID: 31.1.1007/3248/0). They were anesthetized by Isoflurane (Forene, Abbott AG, Baar, Switzerland), decapitated and the brain was extracted. Coronal sections (300 µm-thick), at the level of the primary somatosensory (SSp) cortex, were then cut on a vibrating-blade microtome (Leica VT1200s; Leica Biosystems, Nussloch, Germany) into a cold slicing medium (Nashmi et al. 2002) containing (in mM): 135 N-Methyl-D-glucamine (NMDG), 0.5 $CaCl_2$, 20 choline bicarbonate, 10 glucose, 1 KCl, 1.2 KH_2PO_4, 1.5 $MgCl_2$ (NMDG was first dissolved and then titrated to pH 7.4 with HCl). Following the slicing, tissue was left to recover at 37°C for 1 h and then kept at room temperature (RT), until use, in artificial cerebrospinal fluid (ACSF) containing (in mM): 2.4 $CaCl_2$, 10 glucose, 5 KCl, 1.2 KH_2PO_4, 130 NaCl, 20 $NaHCO_3$, and 1.3 $MgSO_4$ aerated with carbogen (95% O_2 and 5% CO_2). During the recovery period and the time left at RT, 1 mM of kynurenic acid was added to the ACSF. Individual slices were then transferred to a thermoregulated (32°C) recording chamber placed on the stage of an upright microscope (Axioskop, Zeiss, Oberkochen, Germany) equipped with an infrared camera (TILL-Photonics) and a mercury lamp (HBO 100, Zeiss) as well as selective filter sets (filter sets 20 and 38, Zeiss) for fluorescent cell identification. Slices were maintained immersed and were continuously superfused (4–5 mL/min.) with ACSF bubbled with 95% O_2 and 5% CO_2.

Electrophysiological Recordings

Recordings were performed on cells located in cortical L6b (Fig. 1A). This layer is defined as a thin and compact band of neurons lying immediately above the white matter (WM) of the corpus callosum, in the deepest part of the gray matter, below the layer 6a (Valverde et al. 1989; Clancy and Cauller 1999; Reep 2000). In our experiments, such a compact cell layer could be identified under infrared microscopy and neurons therein were preferably recorded the closest to the WM/L6b boundary. Regarding the electrophysiological experiments on GAD67-GFP (line G42) transgenic mice, fluorescent cells in the L6b were first

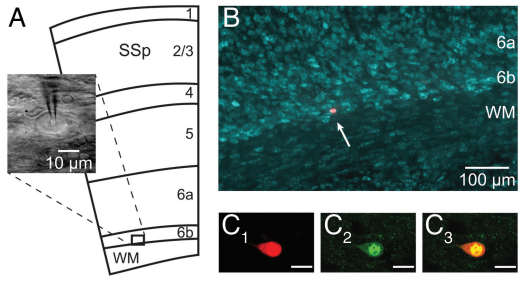

Figure 1. Recordings in L6b. (A) Schematic representation (adapted from the Allen Mouse Brain Atlas; mouse.brain-map.org) of the different layers of the primary somatosensory cortex (SSp) and the underlying white matter (WM), together with an infrared microscopy image of a neuron recorded in this study. (B) Localization of an Alexa Fluor dye-injected neuron in layer 6b (arrow) with fluorescent Nissl counterstaining. (C1–3) Confocal snapshot images of a L6b cell recorded in a GAD67-GFP (line G42) transgenic mouse, showing Alexa Fluor dye-injected fluorescence (C1) and GFP fluorescence (C2) colocalized (C3) in the same cell. Scale bar in C1–3: 10 µm.

visualized with a selective filter set for GFP (filter set 38, Zeiss). Once a GFP-positive cell was selected, it was visualized with infrared illumination and recorded as described below.

The recordings were performed in the whole-cell configuration in either current-clamp or voltage-clamp mode (Uschakov et al. 2011) using an Axopatch 200A amplifier (Molecular Devices, Sunnyvale, CA, USA) and pClamp 10.0 software (Molecular Devices). Patch pipettes (7–12 MΩ for current-clamp and 4–5 MΩ for voltage-clamp) were pulled on a DMZ universal puller (Zeitz-Instruments, Munich, Germany) from borosilicate glass capillaries (GC150F-10, Harvard Apparatus, Holliston, MA, USA) and filled with an intrapipette solution containing (in mM): 3 ATP, 0.1 BAPTA, 0.1 GTP, 10 HEPES, 4 KCl, 126 $KMeSO_4$, 5 $MgCl_2$, 8 phosphocreatine disodium salt, pH 7.3 (285–300 mOsm). In order to validate the colocalization of the recorded cell with the GFP-positive one and allow for a subsequent morphological analysis, Alexa Fluor 555 hydrazide (200 μM; Molecular Probes by Life Technologies, Carlsbad, CA, USA) was generally added to the intrapipette solution. The database for the present study consisted of 65 L6b FS cells. Membrane potential, measured immediately after obtaining whole-cell configuration, was (mean ± SEM) −58.7 ± 0.8 mV ($n = 61$). Membrane potential values were not compensated for junction potential (estimated at −9.6 mV; Eggermann et al. 2003). In several experiments, synaptic transmission was blocked by either adding TTX (10^{-6} M) to the ACSF or increasing its magnesium and lowering its calcium concentration (respectively, 10 mM Mg^{2+} and 0.1 mM Ca^{2+}).

Since no qualitative differences in either intrinsic properties, synaptic activity or the effects of transmitters were observed between the cells recorded from wild type or from the GAD67-GFP (line G42) transgenic mice, data from these 2 mouse strain lines were pooled.

Synaptic Activity Recordings and Analysis

Postsynaptic currents (PSCs) were recorded using voltage-clamp mode. During these experiments, access resistance (10–20 MΩ) was monitored regularly and recordings were discarded if it varied more than 20% during an experiment. In order to investigate the nature of the PSCs, either IVs in ACSF (holding membrane potential $V_h = -60$ mV; 1 s-long steps between −100 and −20 mV) or IVs in the absence or the presence of DNQX (holding membrane potential $V_h = -60$ mV; 9.5 s-long steps at −80, −60, and −40 mV) were performed.

To characterize the effect of hcrt/orx on FS L6b neurons, spontaneous (sPSCs) or miniature (mPSCs) postsynaptic currents were recorded ($V_h = -60$ mV; 10 s-long sweeps) in ACSF or in presence of TTX, respectively. The amplitude and the frequency of the PSCs were then analyzed with a custom-written software (Detector, Dr J.R. Huguenard, Stanford University, Stanford, CA, USA) in which individual events were detected with a threshold-triggered process from a sweep of 10 s both before bath-application and during the maximal effect of the transmitter (due to the important decrease in the number of PSCs in the presence of TTX, 3 successive sweeps of 10 s each were analyzed in TTX experiments). Two detection criteria, namely the threshold and the duration of the trigger, were adjusted to ignore electrical noise and allow maximal discrimination of PSCs. In both conditions (ACSF and TTX), each event detected before application of the transmitter was checked visually in order to avoid artifactual detection (i.e., an event which did not show a typical PSC waveform) and to optimize and validate the adjustment of the program parameters.

For each cell, frequency and mean amplitude of the same number of detected events ($n = 250$) before application and during the maximal effect of the transmitter were calculated and plotted as scatter plots for each condition (ACSF and TTX). The average of frequencies and mean amplitudes of PSCs obtained were plotted as histograms. Changes in cumulative PSC interevent interval and amplitude distributions were also analyzed. Data are presented as mean ± SEM. Statistical analyses were carried out using either unpaired two-tail *t*-test for analyses involving comparison of means or Kolmogorov–Smirnov (KS) test (XLStat, Addinsoft, France) to compare cumulative distributions. Statistical significance was set to $P < 0.01$.

Chemicals

The peptide hypocretin1/orexinA (hcrt1/orxA; Bachem, Bubendorf, Switzerland) was used exclusively in the present study since it is known that hcrt1/orxA peptide is as potent as hypocretin2/orexinB (hcrt2/orxB) on OX2R but more active than hcrt2/orxB on OX1R (Sakurai et al. 1998). For brevity, hcrt1/orxA will be referred to as hcrt/orx. Noradrenaline, carbachol, and neurotensin were all obtained from Sigma-Aldrich (Buchs, Switzerland), while AP5, DNQX, and bicuculline were obtained from Tocris Bioscience (Tocris Bioscience, Bristol, UK), and tetrodotoxin (TTX) from Latoxan (Latoxan, Valence, France). All the drugs were bath-applied.

Histology

Following electrophysiological recordings, a subset of slices with only 1 or 2 dye-injected cells were fixed in a solution of 4% paraformaldehyde for 1–2 h. Slices were then counterstained with NeuroTrace 435/455 blue-fluorescent Nissl stain (Molecular Probes by Life Technologies) to confirm the location of Alexa Fluor-filled neurons in L6b (Fig. 1*B*). For that purpose, after washing in PBS, the slices were incubated twice for 2 h at RT, first in PBS–Triton 0.3% and then in NeuroTrace 1/100 in PBS–Triton 0.3%. After an overnight washing step in PBS, the slices were mounted in FluorSave (Calbiochem) and coverslipped. Images were acquired on an inverted epifluorescence microscope (Nikon Eclipse Ti, Nikon Instruments, Melville, NY, USA) using a 10× magnification objective.

In experiments with transgenic mice, the colocalization of GFP and the Alexa Fluor dye in the recorded cell was always verified at the end of the recording under microscope while the slice was still in the recording chamber. To confirm this colocalization, a subset of dye-injected GFP-positive neurons were fixed and counterstained as described above and snapshot images were acquired (Fig. 1*C1–C3*) using a confocal laser scanning microscope (Zeiss LSM700, Zeiss).

Neurolucida Reconstruction and Morphological Analysis

Alexa Fluor-filled neurons were imaged using a confocal laser scanning microscope (Zeiss LSM700, Zeiss). Confocal image stacks were acquired at 3 different magnifications (20×, 40×, and 63×) to cover the entire dendritic arborization. Dendritic and axonal trees were then reconstructed in 3D from the confocal stacks with Neurolucida 11 software (MBF Bioscience, Williston, VT, USA). Once the tracing was completed, several somatodendritic and axonal features were analyzed using Neurolucida Explorer 11 software (MBF Bioscience). The reconstructions of neurons were aligned to have the WM/L6b boundary parallel to the *x*-axis. Only neurons with minimal extracellular dye leakage and with a total axonal length above 1.0 mm were considered. Five somatic parameters were quantified: the cell body perimeter and its area, the maximum and minimum ferets as well as the aspect ratio.

Max/min ferets were defined, respectively, as the longest/smallest diameter of the soma, measured between two parallel tangential lines drawn along the soma boundaries (as if measured with a caliper). The aspect ratio, defined by the ratio of the maximal feret to the minimal feret, gives an indication about the elongation of the cell body. In order to investigate the dendritic arborization, the following parameters were quantified: the number of primary dendrites, the total dendritic length, the number of nodes, the dendritic branching frequency (i.e., number of nodes/100 µm) and the ratio of the total dendritic length to the total dendritic surface. In order to further analyze the spatial distribution of the dendrites, a Sholl analysis and a polar histogram were also performed. The Sholl analysis, used to represent the dendritic density around the cell body, was expressed as a fraction of the total dendritic length contained in a series of spheres centered at the centroid of the soma with incremental radii (100, 200, and 300 µm). The polar histogram, on the other hand, describes the overall orientation of the dendritic processes in which their 3D reconstruction was reduced to a 2D polar histogram with dendritic lengths plotted, in bins, as a function of direction. The dendritic arborization around the soma was indeed divided in 120 bins of 3° with cubic spline smoothing for each dendritic reconstruction. The average of the dendritic reconstructions of the whole set of cells was calculated and a mean polar plot was obtained with Statgraphics Centurion XVII (Statpoint Technologies, Warrenton, VA, USA) in which the 0–180° axis was parallel to the WM/L6b boundary. On the polar plot, processes pointing to 90° were oriented toward the pial surface whereas those directed to 270° were oriented toward the white matter. In order to characterize the axonal arborization and its spatial distribution, a procedure similar to the one outlined above for the dendritic trees, was applied. Each parameter is presented as mean ± SEM.

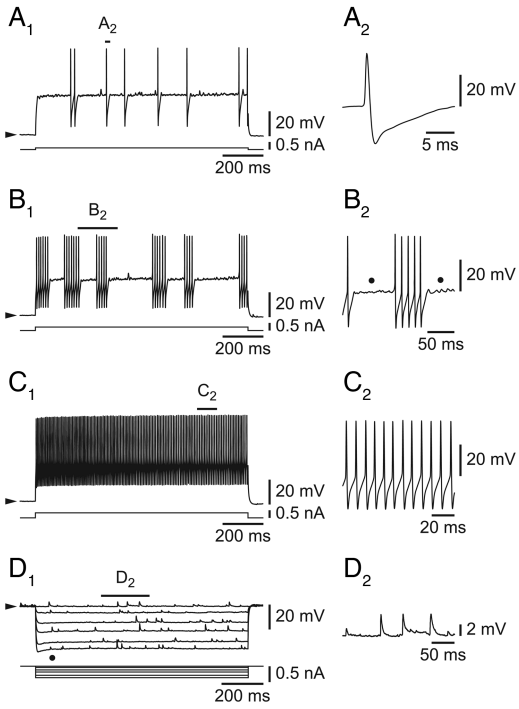

Figure 2. Intrinsic properties of L6b FS cells. (*A1–C1*) Increasing amplitudes of depolarizing steps leading from irregular firing (*A1*) to clustering/stuttering (*B1*) and to high-frequency tonic firing (*C1*). (*D1*) Hyperpolarizing pulses reveal an inward rectification (dot) and spontaneous synaptic activity. (*A2*) Typical FS major after-hyperpolarization, enlarged from *A1*. (*B2*) Cluster of action potentials and subthreshold oscillations (dots), enlarged from *B1*. (*C2*) Fast tonic activity with little adaptation, enlarged from *C1*. (*D2*) Spontaneous synaptic activity, enlarged from *D1*. Filled arrowheads on the left side of electrophysiological traces (on this and the following figures) indicate that recordings are made at resting potentials.

Results

Whole-cell recordings were performed on FS neurons in L6b ($n = 65$) of the mouse SSp cortex (Fig. 1*A*,*B*). About half of the recordings ($n = 30$) was obtained from transgenic GAD67-GFP (line G42) mice (Fig. 1*C1–C3*; see Materials and Methods), while the rest was obtained from wild-type C57Bl/6 mice.

Intrinsic Properties and Spontaneous Synaptic Activity of L6b FS Cells

Fast spiking neurons in L6b of the SSp cortex did not differ from FS cells in other cortical regions (McCormick et al. 1985; Connors and Gutnick 1990; Ascoli et al. 2008) as illustrated in Figure 2. Challenged by a small depolarizing step, they fired in an irregular way (Fig. 2*A1*), with action potentials typically followed by a deep single after-hyperpolarization (Fig. 2*A2*). With increasing amplitude of stimulation, they typically showed a clustering of the action potentials (Fig. 2*B1*, enlarged in 2*B2*), in a pattern previously described as "stuttering" (Ascoli et al. 2008) as well as subthreshold membrane potential oscillations (Fig. 2*B2*, dots). Finally, at an even higher amplitude of stimulation, the cells discharged tonically with little adaptation (Fig. 2*C1*, enlarged in 2*C2*) at a high frequency (107.8 ± 6.0 Hz; range 50.3–195.1 Hz; $n = 35$). These cells also presented a small voltage- and time-dependent inward rectification (Fig. 2*D1*, dot) compatible with the presence of an I_h current.

As illustrated in Figure 2*D1–2*, the L6b FS cells, while usually displaying no spontaneous action potentials at rest, always exhibited a very high level of spontaneous synaptic activity. This activity consisted of EPSPs as demonstrated with the following arguments. First, in voltage-clamp mode, only inward synaptic currents could be recorded ($n = 5/5$; holding potentials ranging from −100 to −20 mV, $n = 4$, and −100 to −30 mV, $n = 1$) and outward currents were never unmasked (not shown). Second, as illustrated in Figure 3, these inward synaptic currents depended on AMPA/kainate glutamatergic transmission as they were completely (Fig. 3, middle panel) but reversibly (Fig. 3, right panel) blocked by the AMPA/kainate receptor antagonist DNQX ($n = 5/5$, at 2×10^{-5} M) at 3 different holding potentials (−80, −60, and −40 mV). In contrast, neither AP5 ($n = 3/3$), an NMDA antagonist (applied at 5×10^{-5} M), nor bicuculline ($n = 2/2$), a $GABA_A$ receptor antagonist (applied at 10^{-5} M), had any effect (not shown). These data therefore suggest an absence of spontaneous IPSPs in these L6b FS cells in our conditions.

Hcrt/orx Increases Spontaneous Excitatory Activity in L6b FS Cells

We next tested the effect of hcrt/orx on L6b FS cells ($n = 53$) in either current-clamp (CC) or voltage-clamp (VC) mode. In CC mode, when neurons were challenged with hcrt/orx (at 10^{-6} M), there was nearly always ($n = 36/37$) a large increase of spontaneous EPSPs as illustrated in Figure 4*A* (enlarged in 4*B1* and 4*B2*). In some cells showing this increase of EPSPs, there was an associated membrane depolarization (3.2 ± 0.5 mV; $n = 15/36$), whereas in others no membrane potential deflection could be observed ($n = 21/36$). Hcrt/orx, in contrast, had no effect when applied in

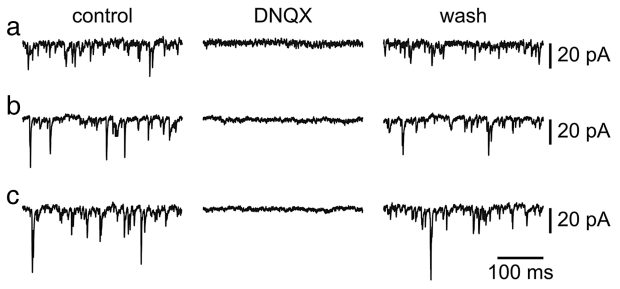

Figure 3. Spontaneous excitatory synaptic potentials of L6b FS cells. (*control*) Spontaneous synaptic activity in a control ACSF, at different holding potentials (−40, −60 and −80 mV, in a, b, and c, respectively). (*DNQX*) Suppression of synaptic activity in the presence of DNQX. (*wash*) Return of synaptic activity following DNQX washout.

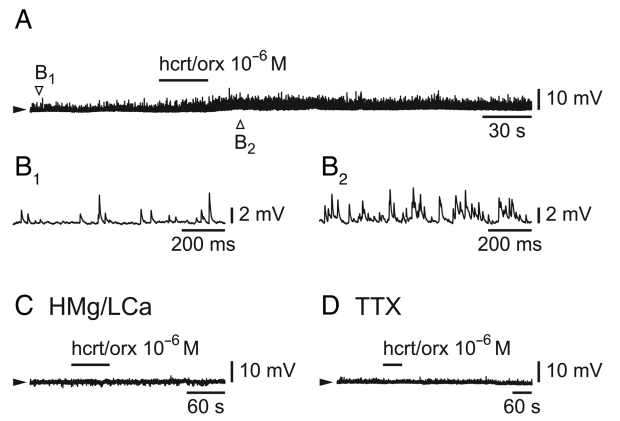

Figure 4. Hcrt/orx increases spontaneous synaptic potentials in L6b FS cells. (*A–B*) Effect of a brief bath-application of hcrt/orx (*A*) with enlargement of synaptic activity before application (*B1*) and during the maximal effect of hcrt/orx (*B2*). (*C*) Absence of effect of hcrt/orx in the presence of a high Mg/low Ca ACSF. (*D*) Absence of effect of hcrt/orx in the presence of TTX.

the presence of either a high Mg/low Ca solution (Fig. 4C; $n = 3/3$) or a TTX-containing ACSF (Fig. 4D; $n = 2/2$).

In order to evaluate the effect of hcrt/orx more precisely on L6b FS cells, it was then tested at 10^{-6} M in the VC mode. As shown in Figure 5A1, hcrt/orx strongly increased the occurrence of spontaneous synaptic currents ($n = 15/16$) in a reversible manner. This effect was entirely explained by a significant increase in the frequency of the synaptic currents with no effect on their amplitude (Fig. 5A2–A5). Indeed, a significant change in interevent interval cumulative distributions ($p_{(KS)} = 10^{-3}$, $n = 9$; Fig. 5A4) together with a significant increase in mean frequencies (from 42.0 ± 4.5 to 100.7 ± 10.7 Hz, $p_{(t\text{-test})} = 2.6 \times 10^{-5}$, $n = 9$; histogram in Fig. 5A4) were observed, whereas no significant change was seen in either amplitude cumulative distributions ($p_{(KS)} = 1.0$, $n = 9$; Fig. 5A5) or mean amplitudes (from 8.8 ± 0.5 to 8.7 ± 0.7 pA, $p_{(t\text{-test})} = 0.88$, $n = 9$; histogram in Fig. 5A5).

We next considered the effect of hcrt/orx in the presence of TTX at 10^{-6} M. In this condition, as illustrated in Figure 5B1 (left panel), some residual synaptic activity could still be recorded, indicating the presence of miniature synaptic currents, but this activity did not appear to be sensitive to hcrt/orx ($n = 5/5$; Fig. 5B1, middle panel), thereby suggesting that the effect was presynaptic. This was confirmed by analyzing further the results in presence of TTX (Fig. 5B2–B5) which indeed showed an absence of effect of hcrt/orx on interevent interval cumulative distributions ($p_{(KS)} = 1.0$, $n = 5$; Fig. 5B4), mean frequencies (from 20.5 ± 6.7 to 20.3 ± 6.1 Hz, $p_{(t\text{-test})} = 0.99$, $n = 5$; histogram in Fig. 5B4), amplitude cumulative distributions ($p_{(KS)} = 1.0$, $n = 5$; Fig. 5B5) as well as on mean amplitudes (from 5.6 ± 0.7 to 5.5 ± 0.9 pA, $p_{(t\text{-test})} = 0.94$, $n = 5$; histogram in Fig. 5B5).

Altogether the data suggest a presynaptic action of hcrt/orx but not on axon terminals impinging on L6b FS cells, but rather on neighboring neurons possibly activated directly by hcrt/orx (Bayer et al. 2004).

Postsynaptic Actions of Noradrenaline and Acetylcholine of L6b FS Cells

As a next step, we then tested the effect of 2 other major wake-promoting transmitters on L6b FS cells that had previously responded to hcrt/orx.

We first tested the effect of noradrenaline (from 10^{-5} to 10^{-4} M) and, as illustrated in Figure 6A, the effect was a significant membrane depolarization in 5/6 cells (range 2.1–6.7 mV; $n = 5$) associated in the majority of cases ($n = 3/5$) with the firing of action potentials. In the presence of either a high Mg/low Ca solution (Fig. 6B) or a TTX-containing ACSF (Fig. 6C), noradrenaline (respectively, from 10^{-5} to 2×10^{-5} M and from 10^{-5} to 10^{-4} M), in contrast to hcrt/orx, had still an effect as it induced, in both conditions, a significant membrane depolarization (range 2.7–3.9 mV in 3/3 cells in high Mg/low Ca and range 2.5–5.8 mV in 3/4 cells in TTX). These results indicate a main postsynaptic effect for this transmitter on L6b FS cells.

We then tested the effect of the cholinergic agonist, carbachol (from 10^{-5} to 10^{-4} M). As illustrated in Figure 7A, as for noradrenaline, the effect was a significant membrane depolarization (range 3.0–11.6 mV; $n = 5/5$) associated with the firing of action potentials in the majority of cases ($n = 3/5$). In the presence of either a high Mg/low Ca solution (Fig. 7B) or a TTX-containing ACSF (Fig. 7C), carbachol, applied at 10^{-5} or 10^{-4} M had still an effect as it induced a significant membrane depolarization in both cases (range 2.3–2.4 mV in 2/3 cells in high Mg/low Ca and range 1.7–4.2 mV in 3/4 cells in TTX). These results indicate a main postsynaptic effect for acetylcholine on L6b FS cells as was the case for noradrenaline.

Neurotensin Effect on L6b FS Cells

We finally tested the effect of neurotensin, a transmitter which is colocalized in hcrt/orx neurons (Furutani et al. 2013) and which was shown to promote high-frequency cortical rhythms by an action on basal forebrain cholinergic neurons (Cape et al. 2000). When it was applied (from 5×10^{-7} to 2×10^{-6} M) on cells that had previously responded to hcrt/orx, it induced a membrane depolarization in 5/7 tested cells (range 2.7–8.5 mV; $n = 5$; Fig. 8A) accompanied in most cells ($n = 4/5$) by the firing of action potentials. This depolarizing effect was however absent when neurotensin was applied in either a high Mg/low Ca solution (Fig. 8B; $n = 3/3$) or in the presence of TTX (Fig. 8C; $n = 3/3$). These results suggest that the effect of neurotensin must be indirect in this case, in contrast to what was observed for noradrenaline and acetylcholine.

Neurolucida Reconstructions of L6b FS Neurons

In order to analyze the morphology of the L6b FS neurons, the recorded cells were injected with a fluorescent red dye, Alexa Fluor 555 hydrazide, and then reconstructed using confocal microscopy and Neurolucida software, as illustrated in Figure 9A1 and A2. As FS cells are generally classified as basket or chandelier

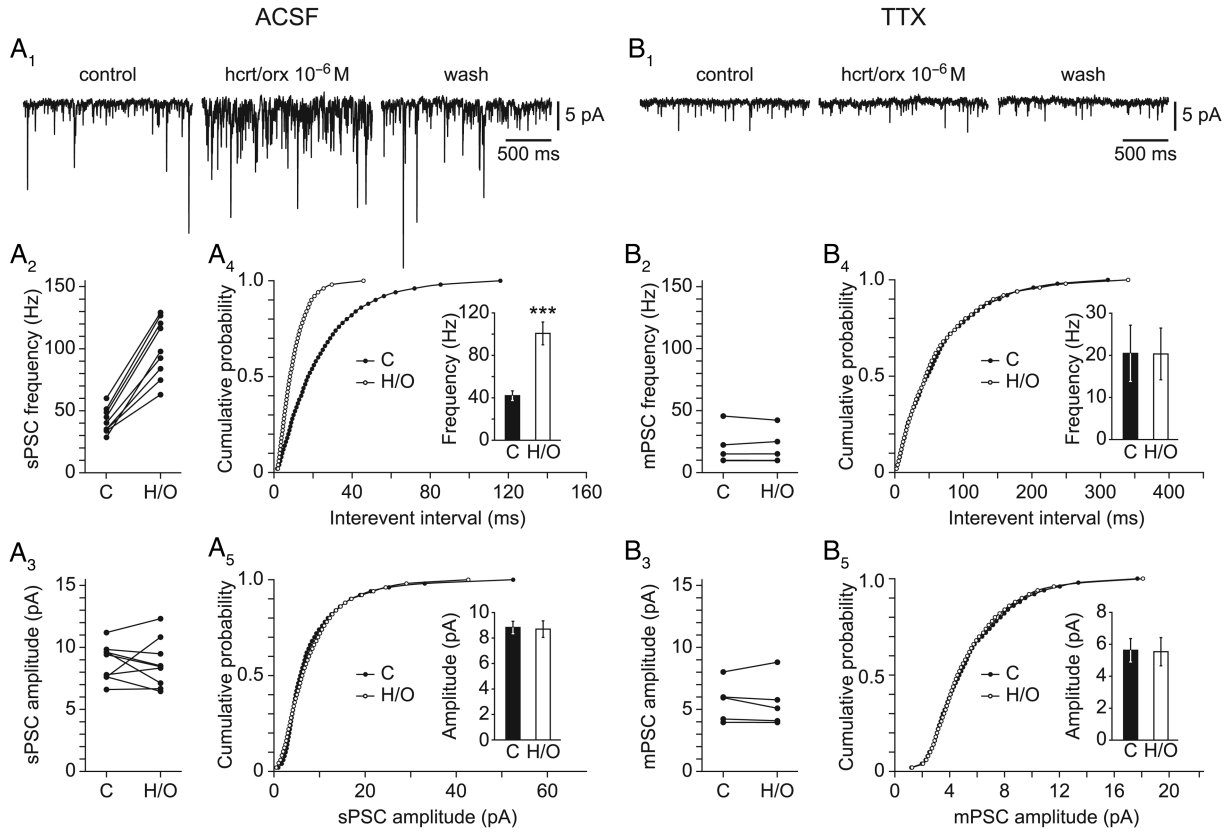

Figure 5. Hcrt/orx increases spontaneous synaptic currents in L6b FS cells. (*A1*) Effect of hcrt/orx on spontaneous synaptic activity, in normal ACSF, with panels illustrating control (left), effect (middle), and wash (right). (*A2–3*) Scatter plots of results of control (C) versus hcrt/orx (H/O) with respect to synaptic current frequencies (*A2*) and amplitudes (*A3*). (*A4–5*) Cumulative distributions of interevent interval (*A4*) and amplitude (*A5*) together with histograms for mean frequencies and amplitudes in control (C) versus hcrt/orx (H/O). (*B1–5*) Same as *A1–5* but in the presence of TTX. Bars in histograms illustrate the mean ± SEM and significant differences are marked by 3 asterisks ($P < 0.01$).

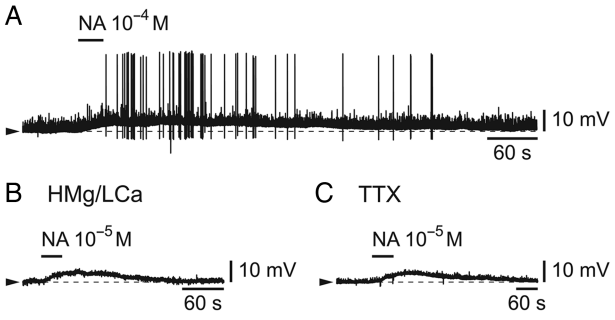

Figure 6. Noradrenaline depolarizes and excites L6b FS cells. (*A*) Depolarizing effect of a brief bath-application of noradrenaline (NA). (*B*) Depolarizing effect of NA in the presence of a high Mg/low Ca ACSF. (*C*) Depolarizing effect of NA in the presence of TTX.

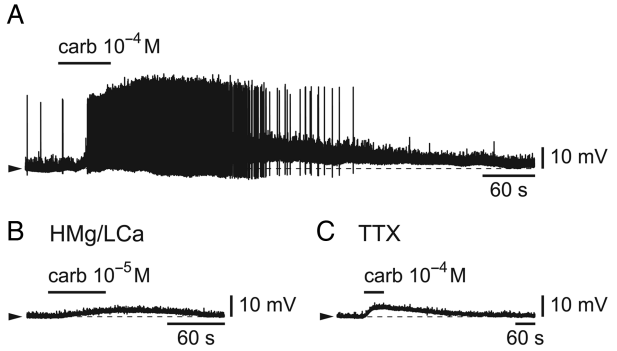

Figure 7. Carbachol depolarizes and excites L6b FS cells. (*A*) Depolarizing effect of a brief bath-application of the cholinergic agonist, carbachol (carb). (*B*) Depolarizing effect of carbachol in the presence of a high Mg/low Ca ACSF. (*C*) Depolarizing effect of carbachol in the presence of TTX.

cells mainly on the basis of their axonal configuration, only neurons whose axon could be followed for more than 1 mm were included in these analyses. As a consequence of this condition, artifacts due to the truncation of processes, known to occur during the slicing procedure, are minimized, thus leading to neurons with a concomitant better integrity of their dendritic processes. Four cells satisfied this criterion and their morphological characteristics are summarized in Table 1.

These L6b FS cells appeared multipolar with 4–7 primary dendrites radiating in all directions (Fig. 9*A1* and *A2*). Their soma appeared fusiform (elongation 2.0 ± 0.4 μm) with mean feret diameters of, respectively, 18.9 ± 2.6 and 9.9 ± 0.9 μm. They had extensive dendritic and axonal arborizations (respective mean length 2323.3 ± 214.2 and 3239.2 ± 952.9 μm) both running beyond 300 μm away from the soma, according to the Sholl analyses. Dendritic trees were smooth (see inset in Fig. 9*A1*) with a branching frequency of 1.1 ± 0.2 nodes/100 μm and the main fraction of dendritic arborization (94.4%) was restricted to a 200 μm radius around their soma with no preferential orientation (see the

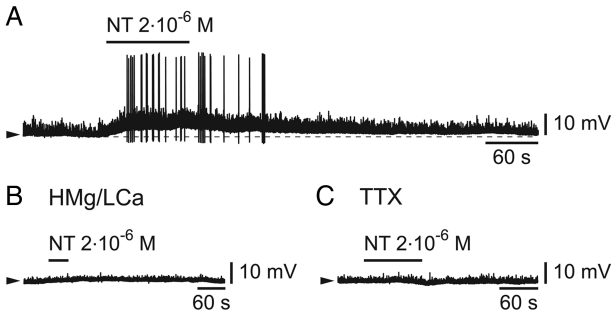

Figure 8. Neurotensin depolarizes and excites L6b FS cells. (*A*) Effect of a brief bath-application of neurotensin (NT). (*B*) Absence of effect of NT in the presence of a high Mg/low Ca ACSF. (*C*) Absence of effect of NT in the presence of TTX.

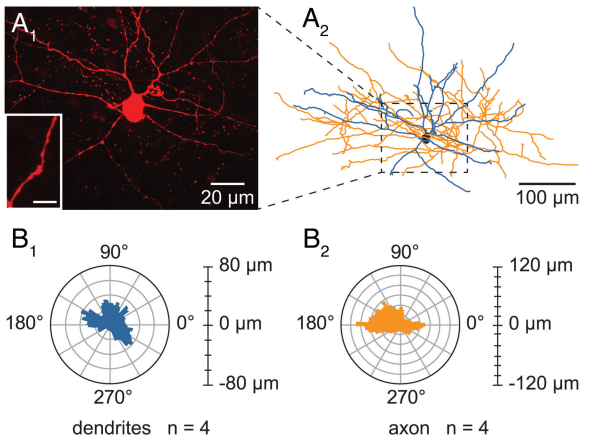

Figure 9. Morphology of the recorded L6b FS cells. (*A1–2*) Representative example of the morphology of a L6b FS cell. (*A1*) Confocal maximum projection image obtained from an image stack of a L6b FS recorded cell and enlargement of a smooth dendrite (lower left inset). Scale bar for the inset: 10 µm. (*A2*) Neurolucida reconstruction from the confocal image stack of the L6b FS cell illustrated in *A1*. (*B1–2*) Polar histograms representing the dendritic (*B1*) and axonal (*B2*) orientations of the 4 L6b FS reconstructed cells. In each polar plot, the radius depicts the average arborization length of the 4 reconstructed cells. The 0–180° axis is parallel to the WM/L6b boundary. Processes pointing to 90° were oriented towards the pial surface whereas those directed to 270° were oriented toward the white matter of the corpus callosum.

dendritic polar plot, Fig. 9*B1*). Axons also arborized mainly (95.2%) within a 200 µm radius around the cell body but, in contrast to the dendrites, they presented a rather horizontal orientation (see axonal polar plot Fig. 9*B2*) with a branching frequency of 1.3 ± 0.1 nodes/100 µm. The axonal arborization of these reconstructed cells was compatible with them being basket cells rather than chandelier cells, as no vertical rows of boutons, characteristic of chandelier cells, were ever observed at the terminal portions of their axon.

Discussion

In a previous study in rat brain slices, we have shown that in the neocortex only L6b neurons were directly sensitive to the wake-promoting transmitter hcrt/orx (Bayer et al. 2004), a result later confirmed in mice (Wenger et al. 2010). Here, in mouse cortical brain slices, we now describe a set of L6b GABAergic FS cells that are indirectly excited by hcrt/orx and neurotensin and directly depolarized and excited by noradrenaline and acetylcholine, thereby suggesting a possible role for these neurons in promoting cortical high-frequency activity.

Table 1 Morphological parameters of L6b FS cells

Morphological parameters	Mean	SEM
Somatic perimeter (µm)	46.5	4.5
Somatic area (µm^2)	127.2	11.3
Max. feret of the soma (µm)	18.9	2.6
Min. feret of the soma (µm)	9.9	0.9
Somatic elongation	2.0	0.4
Number of primary dendrites	5.5	0.7
Total dendritic length (µm)	2323.3	214.2
Number of dendritic nodes	24.5	1.9
Dendritic branching frequency (nodes/100 µm)	1.1	0.2
Dendritic length/dendritic surface	0.7	1.3×10^{-5}
Dendritic Sholl (0–100 µm) (%)	58.1	2.7
Dendritic Sholl (100–200 µm) (%)	36.3	2.8
Dendritic Sholl (200–300 µm) (%)	5.4	2.1
Dendritic Sholl (>300 µm) (%)	0.2	0.2
Total axonal length (µm)	3239.2	952.9
Number of axonal nodes	40.3	12.9
Axonal branching frequency (nodes/100 µm)	1.3	0.1
Axonal length/axonal surface	1.6	5.1×10^{-3}
Axonal Sholl (0–100 µm) (%)	58.2	7.9
Axonal Sholl (100–200 µm) (%)	37.0	5.1
Axonal Sholl (200–300 µm) (%)	4.5	2.9
Axonal Sholl (>300 µm) (%)	0.3	0.3

Each parameter is given as a mean ± SEM of the cells reconstructed according to the criterion described in Materials and Methods section ($n = 4$).

The neurons in the present study were identified as being in L6b by their location within a thin layer of packed cells lying immediately above the white matter of the corpus callosum, in the deepest part of the gray matter (Valverde et al. 1989; Clancy and Cauller 1999; Reep 2000). Their identification was first done visually under infrared microscopy during the electrophysiological recordings (see Materials and Methods section) and then by confirming the location of a subset of dye-filled cells using a fluorescent Nissl stain procedure. Their location corresponded to that of the neurons of the subplate that survive into adulthood (Valverde et al. 1989; Clancy and Cauller 1999; Reep 2000; Watakabe et al. 2007; Hoerder-Suabedissen et al. 2009).

The L6b neurons studied here were characterized as fast spiking (FS) GABAergic neurons with basket-like characteristics, based on their electrophysiological properties, neurotransmitter content, and morphological reconstruction.

With respect to electrophysiology, their identification as FS cells relied on several lines of evidence that include a rather brief action potential followed by a single deep after hyperpolarization, the clustering of action potentials or "stuttering" (as seen in some other FS cortical cells; Ascoli et al. 2008), the high-frequency subthreshold oscillations between clusters and, ultimately, their high-frequency tonic firing with little adaptation when challenged with stronger depolarizing current steps (for review, see Ascoli et al. 2008).

Early on, FS cells were suggested to be GABAergic (McCormick et al. 1985) and later were actually identified as a subtype of cortical GABAergic neurons (for reviews, see Ascoli et al. 2008; Rudy et al. 2011; DeFelipe et al. 2013). The L6b FS cells recorded here were indeed GABAergic as evident from their recording in GAD67-GFP mice. They were also, most probably, parvalbumin-positive cells. Indeed, parvalbumin has been identified as an additional marker in most GABAergic FS cells (Kawaguchi and

Kubota 1998) while being mostly absent in other cortical GABAergic interneurons (for recent review, Rudy et al. 2011). In addition, about half of the L6b FS recordings here were actually obtained in GAD67-GFP (line G42) mice in which GFP-positive cells had been identified as FS parvalbumin-positive cells (Chattopadhyaya et al. 2004; Xu and Callaway 2009). Finally, a recent study in mouse cortical brain slices of L6b GABAergic cells using unsupervised clustering based on electrophysiological, molecular, and morphological parameters, described a class of cells similar to that of the present study which was indeed parvalbumin positive (Perrenoud et al. 2013).

Cortical FS-PV cells have been recently determined to fall into only one of two different morphological classes, chandelier and basket cells (Rudy et al. 2011). In the present study, the Neurolucida reconstructions that were carried out on injected neurons indicated that they were not of the chandelier type but rather of the basket cell type. Indeed, none of the reconstructed cells displayed visible vertical axon cartridges, a hallmark feature of chandelier axon (Kawaguchi 1995; Xu and Callaway 2009). In addition, it is noteworthy that chandelier cells are quite rare and that most of the GFP-positive cells of the transgenic mouse line used here had been described previously as basket cells (Chattopadhyaya et al. 2004; Xu and Callaway 2009).

The L6b FS cells of the present study were strongly activated by hcrt/orx, an effect which was always indirect. This is suggested first by the evidence that hcrt/orx increased the frequency of spontaneous excitatory PSCs, which are conspicuous in these cells (while inhibitory PSCs are absent as evident in DNQX), without increasing their amplitude. It is confirmed by the absence of hcrt/orx effect on miniature synaptic current amplitude in the presence of TTX. The absence, in that latter condition, of hcrt/orx effect on miniature synaptic current frequency, suggests however that it is not due to action on glutamatergic terminals, but rather on neighboring cells activated by the peptide. These results stand in contrast to other studies of hcrt/orx presynaptic excitatory effects in the cortex that have shown an increase in miniatures and thus, a modulatory presynaptic effect on glutamatergic terminals (Lambe and Aghajanian 2003; Aracri et al. 2015). Finally, one must stress that given the reported prevalence of electrical coupling among FS neurons elsewhere in the cortex (Galarreta and Hestrin 1999; Gibson et al. 1999), one cannot exclude that some of the spontaneous activity reported here was actually due to such coupling.

Based on our previous studies that have demonstrated an exclusive postsynaptic action of hcrt/orx in L6b neurons in rat brain slices (Bayer et al. 2004) as well as in mice (Wenger et al. 2010), a possible interpretation is that the increased EPSPs recorded here originate from contiguous glutamatergic L6b neurons that are directly (postsynaptically) activated by hcrt/orx. The strength of this effect suggests the presence of a tight control of the firing of presumed glutamatergic and secondarily GABAergic neurons in L6b by hcrt/orx. Neurotensin, a neuropeptide which is colocalized in hcrt/orx neurons (Furutani et al. 2013) and which was shown to be able to promote high-frequency cortical rhythms (Cape et al. 2000), could possibly exert a similar control, given that its strong depolarizing and excitatory action on L6b FS neurons is also entirely indirect.

L6b FS cells were also excited by noradrenaline and acetylcholine but, in contrast to hcrt/orx and neurotensin, it was the result of a direct, postsynaptic action. This contention is based on the persistence of depolarizing and/or excitatory responses to these transmitters in conditions of either TTX or synaptic uncoupling. These results are in agreement with numerous studies since the early 80s (for review, see McCormick 1989) which have identified postsynaptic excitatory effects of these transmitters on cortical neurons, including, more recently, effects of noradrenaline on FS neurons (Kawaguchi and Shindou 1998). With respect to acetylcholine, however, the data of the present study seem to be the first to show a postsynaptic depolarizing and excitatory effect on cortical FS neurons. A recent thorough investigation of acetylcholine effects has actually concluded, to the contrary, that FS neurons in the cortex are not directly sensitive to acetylcholine (Gulledge et al. 2007). Nevertheless, it is noteworthy that in the hippocampus, a structure also prone to FS-dependent GBO, FS cells were found to be directly sensitive to acetylcholine (Chiang et al. 2010).

Functionally, one could speculate that the effects of the neurotransmitters on L6b FS neurons described here could contribute to the cortical activation associated with arousal. Fast cortical rhythms and arousal have indeed been known since the early studies of Moruzzi and Magoun (1949) to depend on the influence of the "ascending reticular activating system" even though the exact nature of the system was not understood at that time. Later on, the transmitters implicated in this action, and the pathways containing them, were sorted out and among them, noradrenaline from the locus coeruleus and acetylcholine from the basal forebrain, have been held as prominent players since then (for review, see Jones 2003). More recently, an hypothalamic peptide, hcrt/orx (de Lecea et al. 1998; Sakurai et al. 1998), was found to be a major wake-promoting transmitter and as such to be also involved in enabling the cortical high-frequency rhythms associated with the waking state (for recent reviews, see Siegel and Boehmer 2006; Alexandre et al. 2013; Jones and Hassani 2013; Mahlios et al. 2013; Sakurai 2013; de Lecea and Huerta 2014), including possibly by an action on adrenergic (Horvath et al. 1999) and cholinergic (Eggermann et al. 2001; Burlet et al. 2002; Ishibashi et al. 2015) neurons.

In recent years, many studies have proposed that a network of cortical FS-PV cells plays a major role in the genesis of high-frequency rhythms (Freund 2003; Cardin et al. 2009; Sohal et al. 2009; Hu et al. 2014; Kim et al. 2015) but, with the exception of a recent study concerning acetylcholine (Pafundo et al. 2013), the link between this network and the arousal systems referred to above, has thus far remained elusive. It is thus tempting to speculate that what was observed in the present study bears particular significance. It is indeed noteworthy that hcrt/orx, which in the somatosensory cortex is thought to exert a direct action only in layer 6b (Bayer et al. 2004; Wenger et al. 2010), appears to directly transfer this excitatory action within L6b to that very class of GABAergic neurons, the FS-PV cells, which today is thought to play a central role in the generation of high-frequency rhythms. It is also noteworthy that these L6b FS cells that are sensitive to hcrt/orx, are, at the same time, directly and strongly excited by noradrenaline and acetylcholine. Finally, it is intriguing that the direct effect of acetylcholine on FS cells, as reported here in L6b, appears to be rather unique to this layer, as it was reported to be absent elsewhere in the cerebral cortex (Gulledge et al. 2007).

Altogether these data speak in favor of a potential role of layer 6b on cortical activation but in the absence of knowledge concerning the cortical projections of the L6b FS cells, the mechanisms involved remain unknown.

Funding

This work was supported by the Swiss National Science Foundation (SNSF) (grant number 31003AB_135708). Funding to pay the Open Access publication charges for this article was provided by the Faculty of Medicine, Geneva, Switzerland.

Notes

We thank Dr V. Cvetkovic-Lopes for help in confocal acquisition and Ms G. Gilliéron for help in the histological work. We also thank Dr A. Hoerder-Suabedissen and Dr Z. Molnar for their help in identifying layer 6b, as well as Dr P. Mendez and Dr V. Pascoli for helping with synaptic current analysis. We finally thank Dr P. Mendez for making available Dr Huguenard software for synaptic analysis. *Conflict of Interest:* None declared.

References

Alexandre C, Andermann ML, Scammell TE. 2013. Control of arousal by the orexin neurons. Curr Opin Neurobiol. 23 (5):752–759.

Aracri P, Banfi D, Pasini ME, Amadeo A, Becchetti A. 2015. Hypocretin (orexin) regulates glutamate input to fast-spiking interneurons in layer v of the fr2 region of the murine prefrontal cortex. Cereb Cortex. 25(5):1330–1347.

Arimatsu Y, Ishida M, Kaneko T, Ichinose S, Omori A. 2003. Organization and development of corticocortical associative neurons expressing the orphan nuclear receptor Nurr1. J Comp Neurol. 466(2):180–196.

Ascoli GA, Alonso-Nanclares L, Anderson SA, Barrionuevo G, Benavides-Piccione R, Burkhalter A, Buzsaki G, Cauli B, Defelipe J, Fairen A, et al. 2008. Petilla terminology: nomenclature of features of GABAergic interneurons of the cerebral cortex. Nat Rev Neurosci. 9(7):557–568.

Bayer L, Eggermann E, Saint-Mleux B, Machard D, Jones BE, Muhlethaler M, Serafin M. 2002. Selective action of orexin (hypocretin) on nonspecific thalamocortical projection neurons. J Neurosci. 22(18):7835–7839.

Bayer L, Serafin M, Eggermann E, Saint-Mleux B, Machard D, Jones BE, Muhlethaler M. 2004. Exclusive postsynaptic action of hypocretin-orexin on sublayer 6b cortical neurons. J Neurosci. 24(30):6760–6764.

Burlet S, Tyler CJ, Leonard CS. 2002. Direct and indirect excitation of laterodorsal tegmental neurons by hypocretin/orexin peptides: implications for wakefulness and narcolepsy. J Neurosci. 22(7):2862–2872.

Cape EG, Manns ID, Alonso A, Beaudet A, Jones BE. 2000. Neurotensin-induced bursting of cholinergic basal forebrain neurons promotes gamma and theta cortical activity together with waking and paradoxical sleep. J Neurosci. 20 (22):8452–8461.

Cardin JA, Carlen M, Meletis K, Knoblich U, Zhang F, Deisseroth K, Tsai LH, Moore CI. 2009. Driving fast-spiking cells induces gamma rhythm and controls sensory responses. Nature. 459 (7247):663–667.

Chattopadhyaya B, Di Cristo G, Higashiyama H, Knott GW, Kuhlman SJ, Welker E, Huang ZJ. 2004. Experience and activity-dependent maturation of perisomatic GABAergic innervation in primary visual cortex during a postnatal critical period. J Neurosci. 24(43):9598–9611.

Chiang PH, Yeh WC, Lee CT, Weng JY, Huang YY, Lien CC. 2010. M (1)-like muscarinic acetylcholine receptors regulate fast-spiking interneuron excitability in rat dentate gyrus. Neuroscience. 169(1):39–51.

Chun JJ, Shatz CJ. 1989. Interstitial cells of the adult neocortical white matter are the remnant of the early generated subplate neuron population. J Comp Neurol. 282(4):555–569.

Clancy B, Cauller LJ. 1999. Widespread projections from subgriseal neurons (layer VII) to layer I in adult rat cortex. J Comp Neurol. 407(2):275–286.

Clancy B, Silva-Filho M, Friedlander MJ. 2001. Structure and projections of white matter neurons in the postnatal rat visual cortex. J Comp Neurol. 434(2):233–252.

Connors BW, Gutnick MJ. 1990. Intrinsic firing patterns of diverse neocortical neurons. Trends Neurosci. 13(3):99–104.

DeFelipe J, Lopez-Cruz PL, Benavides-Piccione R, Bielza C, Larranaga P, Anderson S, Burkhalter A, Cauli B, Fairen A, Feldmeyer D, et al. 2013. New insights into the classification and nomenclature of cortical GABAergic interneurons. Nat Rev Neurosci. 14(3):202–216.

de Lecea L, Huerta R. 2014. Hypocretin (orexin) regulation of sleep-to-wake transitions. Front Pharmacol. 5:16.

de Lecea L, Kilduff TS, Peyron C, Gao X, Foye PE, Danielson PE, Fukuhara C, Battenberg EL, Gautvik VT, Bartlett FS, et al. 1998. The hypocretins: hypothalamus-specific peptides with neuroexcitatory activity. Proc Natl Acad Sci USA. 95 (1):322–327.

Eggermann E, Bayer L, Serafin M, Saint-Mleux B, Bernheim L, Machard D, Jones BE, Muhlethaler M. 2003. The wake-promoting hypocretin-orexin neurons are in an intrinsic state of membrane depolarization. J Neurosci. 23(5):1557–1562.

Eggermann E, Serafin M, Bayer L, Machard D, Saint-Mleux B, Jones BE, Mühlethaler M. 2001. Orexins/hypocretins excite basal forebrain cholinergic neurones. Neuroscience. 108 (2):177–181.

Freund TF. 2003. Interneuron diversity series: rhythm and mood in perisomatic inhibition. Trends Neurosci. 26(9):489–495.

Friedlander MJ, Torres-Reveron J. 2009. The changing roles of neurons in the cortical subplate. Front Neuroanat. 3:15.

Furutani N, Hondo M, Kageyama H, Tsujino N, Mieda M, Yanagisawa M, Shioda S, Sakurai T. 2013. Neurotensin co-expressed in orexin-producing neurons in the lateral hypothalamus plays an important role in regulation of sleep/wakefulness states. PLoS One. 8(4):e62391.

Galarreta M, Hestrin S. 1999. A network of fast-spiking cells in the neocortex connected by electrical synapses. Nature. 402 (6757):72–75.

Gibson JR, Beierlein M, Connors BW. 1999. Two networks of electrically coupled inhibitory neurons in neocortex. Nature. 402 (6757):75–79.

Gulledge AT, Park SB, Kawaguchi Y, Stuart GJ. 2007. Heterogeneity of phasic cholinergic signaling in neocortical neurons. J Neurophysiol. 97(3):2215–2229.

Hoerder-Suabedissen A, Wang WZ, Lee S, Davies KE, Goffinet AM, Rakic S, Parnavelas J, Reim K, Nicolic M, Paulsen O, et al. 2009. Novel markers reveal subpopulations of subplate neurons in the murine cerebral cortex. Cereb Cortex. 19 (8):1738–1750.

Horvath TL, Peyron C, Diano S, Ivanov A, Aston-Jones G, Kilduff TS, van den Pol AN. 1999. Hypocretin (orexin) activation and synaptic innervation of the locus coeruleus noradrenergic system. J Comp Neurol. 415(2):145–159.

Hu H, Gan J, Jonas P. 2014. Interneurons. Fast-spiking, parvalbumin(+) GABAergic interneurons: from cellular design to microcircuit function. Science. 345(6196):1255263.

Inan M, Anderson SA. 2014. The chandelier cell, form and function. Curr Opin Neurobiol. 26:142–148.

Ishibashi M, Gumenchuk I, Kang B, Steger C, Lynn E, Molina NE, Eisenberg LM, Leonard CS. 2015. Orexin receptor activation generates gamma band input to cholinergic and serotonergic arousal system neurons and drives an intrinsic Ca(2+)-dependent resonance in LDT and PPT cholinergic neurons. Front Neurol. 6:120.

Jones BE. 2003. Arousal systems. Front Biosci. 8:S438–S451.

Jones BE. 2011. Neurobiology of waking and sleeping. Handb Clin Neurol. 98:131–149.

Jones BE, Hassani OK. 2013. The role of Hcrt/Orx and MCH neurons in sleep-wake state regulation. Sleep. 36(12):1769–1772.

Kanold PO, Luhmann HJ. 2010. The subplate and early cortical circuits. Annu Rev Neurosci. 33:23–48.

Kawaguchi Y. 1995. Physiological subgroups of nonpyramidal cells with specific morphological characteristics in layer II/III of rat frontal cortex. J Neurosci. 15(4):2638–2655.

Kawaguchi Y, Kubota Y. 1993. Correlation of physiological subgroupings of nonpyramidal cells with parvalbumin- and calbindinD28k-immunoreactive neurons in layer V of rat frontal cortex. J Neurophysiol. 70(1):387–396.

Kawaguchi Y, Kubota Y. 1998. Neurochemical features and synaptic connections of large physiologically-identified GABAergic cells in the rat frontal cortex. Neuroscience. 85(3):677–701.

Kawaguchi Y, Shindou T. 1998. Noradrenergic excitation and inhibition of GABAergic cell types in rat frontal cortex. J Neurosci. 18(17):6963–6976.

Kim T, Thankachan S, McKenna JT, McNally JM, Yang C, Choi JH, Chen L, Kocsis B, Deisseroth K, Strecker RE, et al. 2015. Cortically projecting basal forebrain parvalbumin neurons regulate cortical gamma band oscillations. Proc Natl Acad Sci U S A. 112 (11):3535–3540.

Kostovic I, Rakic P. 1980. Cytology and time of origin of interstitial neurons in the white matter in infant and adult human and monkey telencephalon. J Neurocytol. 9(2):219–242.

Lambe EK, Aghajanian GK. 2003. Hypocretin (orexin) induces calcium transients in single spines postsynaptic to identified thalamocortical boutons in prefrontal slice. Neuron. 40(1):139–150.

Lee MG, Hassani OK, Jones BE. 2005. Discharge of identified orexin/hypocretin neurons across the sleep-waking cycle. J Neurosci. 25(28):6716–6720.

Mahlios J, De la Herran-Arita AK, Mignot E. 2013. The autoimmune basis of narcolepsy. Curr Opin Neurobiol. 23 (5):767–773.

Maloney KJ, Cape EG, Gotman J, Jones BE. 1997. High-frequency gamma electroencephalogram activity in association with sleep-wake states and spontaneous behaviors in the rat. Neuroscience. 76(2):541–555.

McCormick DA. 1989. Cholinergic and noradrenergic modulation of thalamocortical processing. Trends Neurosci. 12(6): 215–221.

McCormick DA, Connors BW, Lighthall JW, Prince DA. 1985. Comparative electrophysiology of pyramidal and sparsely spiny stellate neurons of the neocortex. J Neurophysiol. 54(4): 782–806.

Mileykovskiy BY, Kiyashchenko LI, Siegel JM. 2005. Behavioral correlates of activity in identified hypocretin/orexin neurons. Neuron. 46(5):787–798.

Moruzzi G, Magoun HW. 1949. Brain stem reticular formation and activation of the EEG. Electroencephalogr Clin Neurophysiol. 1(4):455–473.

Nashmi R, Velumian AA, Chung I, Zhang L, Agrawal SK, Fehlings MG. 2002. Patch-clamp recordings from white matter glia in thin longitudinal slices of adult rat spinal cord. J Neurosci Methods. 117(2):159–166.

Pafundo DE, Miyamae T, Lewis DA, Gonzalez-Burgos G. 2013. Cholinergic modulation of neuronal excitability and recurrent excitation-inhibition in prefrontal cortex circuits: implications for gamma oscillations. J Physiol. 591(Pt 19):4725–4748.

Perrenoud Q, Rossier J, Geoffroy H, Vitalis T, Gallopin T. 2013. Diversity of GABAergic interneurons in layer VIa and VIb of mouse barrel cortex. Cereb Cortex. 23(2):423–441.

Peyron C, Tighe DK, van den Pol AN, de Lecea L, Heller HC, Sutcliffe JG, Kilduff TS. 1998. Neurons containing hypocretin (orexin) project to multiple neuronal systems. J Neurosci. 18 (23):9996–10015.

Povysheva NV, Zaitsev AV, Gonzalez-Burgos G, Lewis DA. 2013. Electrophysiological heterogeneity of fast-spiking interneurons: chandelier versus basket cells. PLoS One. 8(8):e70553.

Reep RL. 2000. Cortical layer VII and persistent subplate cells in mammalian brains. Brain Behav Evol. 56(4):212–234.

Reep RL, Goodwin GS. 1988. Layer VII of rodent cerebral cortex. Neurosci Lett. 90(1–2):15–20.

Rudy B, Fishell G, Lee S, Hjerling-Leffler J. 2011. Three groups of interneurons account for nearly 100% of neocortical GABAergic neurons. Dev Neurobiol. 71(1):45–61.

Sakurai T. 2013. Orexin deficiency and narcolepsy. Curr Opin Neurobiol. 23(5):760–766.

Sakurai T, Amemiya A, Ishii M, Matsuzaki I, Chemelli RM, Tanaka H, Williams SC, Richardson JA, Kozlowski GP, Wilson S, et al. 1998. Orexins and orexin receptors: a family of hypothalamic neuropeptides and G protein-coupled receptors that regulate feeding behavior. Cell. 92(4):573–585.

Schone C, Apergis-Schoute J, Sakurai T, Adamantidis A, Burdakov D. 2014. Coreleased orexin and glutamate evoke nonredundant spike outputs and computations in histamine neurons. Cell Rep. 7(3):697–704.

Siegel JM, Boehmer LN. 2006. Narcolepsy and the hypocretin system–where motion meets emotion. Nat Clin Pract Neurol. 2(10):548–556.

Sohal VS, Zhang F, Yizhar O, Deisseroth K. 2009. Parvalbumin neurons and gamma rhythms enhance cortical circuit performance. Nature. 459(7247):698–702.

Uschakov A, Grivel J, Cvetkovic-Lopes V, Bayer L, Bernheim L, Jones BE, Muhlethaler M, Serafin M. 2011. Sleep-deprivation regulates alpha-2 adrenergic responses of rat hypocretin/orexin neurons. PLoS One. 6(2):e16672.

Valverde F, Facal-Valverde MV, Santacana M, Heredia M. 1989. Development and differentiation of early generated cells of sublayer VIb in the somatosensory cortex of the rat: a correlated Golgi and autoradiographic study. J Comp Neurol. 290 (1):118–140.

Watakabe A, Ichinohe N, Ohsawa S, Hashikawa T, Komatsu Y, Rockland KS, Yamamori T. 2007. Comparative analysis of layer-specific genes in Mammalian neocortex. Cereb Cortex. 17(8):1918–1933.

Wenger A-L, Bayer L, Cvetkovic-Lopes V, Serafin M, Muhlethaler M. 2011. Indirect effect of hypocretin/orexin on layer 6b fast spiking neurons of mice somatosensory cortex. Program No. 720.07. 2011 Neuroscience Meeting Planner. Washington, DC: Society for Neuroscience, 2011.

Wenger A-L, Bayer L, Cvetkovic-Lopes V, Serafin M, Muhlethaler M. 2010. Layer 6b cortical neurons are excited by serotonin and histamine. Program No. 798.10. 2010 Neuroscience Meeting Planner. San Diego, CA: Society for Neuroscience, 2010.

Whittington MA, Traub RD, Jefferys JG. 1995. Synchronized oscillations in interneuron networks driven by metabotropic glutamate receptor activation. Nature. 373(6515):612–615.

Xu X, Callaway EM. 2009. Laminar specificity of functional input to distinct types of inhibitory cortical neurons. J Neurosci. 29(1):70–85.